PLOS | ONE

RESEARCH ARTICLE

Self-Organized Near-Zero-Lag Synchronization Induced by Spike-Timing Dependent Plasticity in Cortical Populations

Fernanda S. Matias[1]*, Pedro V. Carelli[2], Claudio R. Mirasso[3], Mauro Copelli[2]

1 Instituto de Física, Universidade Federal de Alagoas, Maceió AL 57072-970, Brazil, **2** Departamento de Física, Universidade Federal de Pernambuco, Recife PE 50670-901, Brazil, **3** Instituto de Física Interdisciplinar y Sistemas Complejos, IFISC CSIC-UIB, Campus Universitat de les Illes Balears, E-07122 Palma de Mallorca, Spain

* fernanda@fis.ufal.br

Citation: Matias FS, Carelli PV, Mirasso CR, Copelli M (2015) Self-Organized Near-Zero-Lag Synchronization Induced by Spike-Timing Dependent Plasticity in Cortical Populations. PLoS ONE 10(10): e0140504. doi:10.1371/journal.pone.0140504

Editor: Pedro Antonio Valdes-Sosa, Cuban Neuroscience Center, CUBA

Received: June 24, 2015

Accepted: September 21, 2015

Published: October 16, 2015

Data Availability Statement: All relevant data are within the paper.

Funding: This work was supported by project FIS2012-30634 (Intense@cosyp) from Ministerio de Economia y Competitividad, Espaa and Fondo Europeo de Desarrollo Regional. Coordenação de Aperfeiçoamento de Pessoal de Nível Superior (CAPES, Brazilian project Ciência Sem Fronteiras PVE 88881.068077/2014-01); Conselho Nacional de Desenvolvimento Científico e Tecnológico (CNPq), Fundação de Amparo á Ciência e Tecnologia do Estado de Pernambuco (FACEPE), special programs as Programa de Apoio a Núcleos Emergentes

Abstract

Several cognitive tasks related to learning and memory exhibit synchronization of macroscopic cortical areas together with synaptic plasticity at neuronal level. Therefore, there is a growing effort among computational neuroscientists to understand the underlying mechanisms relating synchrony and plasticity in the brain. Here we numerically study the interplay between spike-timing dependent plasticity (STDP) and anticipated synchronization (AS). AS emerges when a dominant flux of information from one area to another is accompanied by a negative time lag (or phase). This means that the receiver region pulses before the sender does. In this paper we study the interplay between different synchronization regimes and STDP at the level of three-neuron microcircuits as well as cortical populations. We show that STDP can promote auto-organized zero-lag synchronization in unidirectionally coupled neuronal populations. We also find synchronization regimes with negative phase difference (AS) that are stable against plasticity. Finally, we show that the interplay between negative phase difference and STDP provides limited synaptic weight distribution without the need of imposing artificial boundaries.

Introduction

Synchronization by neuronal oscillation is a ubiquitous phenomenon in the brain [1]. It has been reported in many species and in a variety of sensory and motor tasks [2, 3]. In particular, coherent oscillations in the cortex have been related to associative learning as well as working and long-term memory [4–6]. In these synchronized regimes, it is possible to determine the relative phase difference in the activation of the involved areas. In unidirectionally coupled motifs, for example, the relative phase difference is usually positive, which means that the sender population transfers information and activates the receiver population. However, it has been shown that, in the presence of dynamical inhibitory loops in the receiver population, unidirectionally coupled neuronal models may exhibit either positive or negative phase differences

(PRONEM) and FAPESP Center for Neuromathematics (grant # 2013/07699-0, S. Paulo Research Foundation FAPESP). The funders had no role in study design, data collection and analysis, decision to publish, or preparation of the manuscript.

Competing Interests: The authors have declared that no competing interests exist.

[7, 8]. This sender-receiver model [8] has been proposed as a mechanism to explain the reported mismatch between directional influence and negative time delay among regions of the monkey cortex [6, 8, 9].

The counterintuitive situation in which the receiver leads the sender, characterized by a negative phase difference, is called anticipated synchronization (AS) [10–12]. AS can be a stable solution of a sender-receiver (or, equivalently, a master-slave) system, if the receiver is also subject to a negative delayed self-feedback [13–21]. AS has been theoretically and experimentally studied in a number of physical systems [22–29]. Nonetheless, there are few investigation of AS in biological systems [30] as well as in the relation between anticipatory behavior and AS dynamics [31, 32]. In fact, the first observation of AS in a neuronal model was done by Ciszak et al [30]. It was shown that two unidirectionally coupled FitzHugh-Nagumo neuron models driven by white noise can exhibit AS in the presence of a negative delayed self-feedback in the receiver neuron. AS was also verified in other master-slave neuron models due to synaptic delays [33] and depolarization parameters [34]. A biologically plausible model for AS in neuronal systems was studied in [7], using three Hodgkin-Huxley neuron models coupled in a sender-receiver configuration, with the delayed self-feedback replaced by a synaptic loop mediated by an inhibitory neuron [7].

More recently, AS was numerically found between unidirectionally coupled neuronal populations in the presence of dynamical inhibitory loops [8]. It was argued that the reported positive Granger causality and negative phase difference among cortical areas [6, 9] could be the first experimental evidence of AS in the brain [8]. In a nutshell, it was experimentally observed that a brain region A could Granger-cause synchronized activity in a region B, yet the phase difference between the two could be negative [9]. This paradox was only apparent because, as the AS phenomenon clearly shows, temporal differences are not a good proxy for causality. Even a simple neuronal population model could reproduce time differences, coherence and GC spectra of the experimental data [8]. Additionally, it was shown that the time delay (or phase difference) between the master and the slave in the model is a smooth function of the excitatory and inhibitory weights. This means that the synaptic weights mediate transitions from positive time delay, called delayed synchronization (DS) regime, to negative time delay (AS regime).

These results, together with the experimental evidence that the synaptic weights can undergo spike-timing dependent plasticity (STDP) [35–37], open new perspectives in the study of neuronal network dynamics. In fact, the mechanisms relating synchronization and plasticity are still under investigation [38–43]. Based on STDP rules, the time difference between the spikes of pre- and post-synaptic neurons engenders modifications in the synaptic weights. On the one hand, synaptic changes induced by STDP rules can promote a transition between synchronized regimes. On the other hand, a given synchronization regime can strongly influence the relative spike times, and hence the STDP dynamics. Here, we investigate the interplay between STDP and the AS-DS transition. In other words, we study how STDP rules and the synchronization regimes work synergistically to determine the network dynamics.

Initially we study a simple 3-neuron motif which exhibits AS and DS regimes [7]. In the DS regime the master (pre-synaptic) neuron fires a spike before the slave (post-synaptic) neuron, which under STDP rules facilitates long term potentiation (LTP) [36, 44, 45]. In the AS regime the slave neuron fires a spike before the master neuron, contributing to long term depression (LTD). In turn, the increase (or decrease) of the excitatory synaptic weights via LTP (or LTD) generates modifications in the time delay. These successive interactions regulate the functional organization of a simple 3-neuron motif.

Next, we study the effect of STDP in the excitatory synapses between two unidirectionally coupled cortical-like populations which exhibits AS or DS. We investigate how the STDP rules applied at the neuronal level can influence synchronization at the populational level. We show

that the interplay between these two different scales gives rise to emergent properties when compared with the 3-neuron motif. First, STDP and the inhibitory loop provide a new mechanism for near-zero-lag synchronization between distant cortical areas. Second, the AS regime is robust against STDP. Third, the transition from AS to DS can be controlled by the local amount of inhibition in the receiver population. We also show that, together with AS, STDP rules provide synaptic weight distributions that are stable, diverse and limited [46]. Furthermore, in the AS regime, such distributions are comparable to those observed experimentally in the cortex [47–49].

Results

Three-neuron motif

The simplest biophysical neuronal model which exhibits AS is the 3-neuron motif shown in Fig 1(a) [7]. It consists of three identical Hodgkin-Huxley neurons spiking periodically: the master (M), the slave (S), and the interneuron (I), coupled by chemical synapses. They are connected via two excitatory synapses, from M to S (g_{MS}) and from S to I (g_{SI}), as well as an inhibitory synapse from I to S (g_{IS}, see Methods for more details). The time delay $\tau = t^S - t^M$ is defined as the spike timing difference between the S and M neurons. It was shown that without plasticity, this motif may present two phase-locking regimes: DS ($\tau > 0$) and AS ($\tau < 0$), as well as a phase-drift (PD) regime [7]. The membrane potentials of M and S shown in Fig 1(b)–1(d)) illustrate each regime.

In what follows, we apply STDP rules in the excitatory synapse from M (pre-synaptic neuron) to S (post-synaptic neuron). Thus, the excitatory synaptic conductance g_{MS} changes according to the spike timing difference between M and S following Eq 10. Typically, for unidirectionally coupled neurons, the post-synaptic neuron fires after the pre-synaptic neuron (characterizing a DS regime) promoting LTP. However, due to the existence of the AS regime in the 3-neuron motif, the presence of STDP can also cause a decrease of the synaptic weight (LTD).

The effect of STDP in the DS regime causes the synaptic weight g_{MS} to increase via LTP until the imposed upper boundary is reached (see right panel of Fig 1(b)). Although one could expect that larger values of the excitatory synaptic weight would facilitate near-zero-lag synchronization, in our model τ is a monotonically increasing function of g_{MS} (see Fig 1(e)). Therefore, STDP leads to an increase in τ (compare S and S_{STDP} in Fig 1(b)).

In the AS regime the post-pre order of spikes facilitates LTD. When we turn on STDP, the synaptic weight decreases. The final regime depends on the lower boundary g^{min} of the algorithm. If $g^{min} < 6$ nS, the system reaches a PD regime (compare S and S_{STDP} in Fig 1(c)). In the AS regime, both M and S oscillate with a period $T_M = 14.7$ ms, whereas in the PD regime the new period of the slave is 14.1 ms (i.e. it is faster than the master). After a transient time, the synaptic weight g_{MS} oscillates between 0 and 4 nS (see right panel of Fig 1(c)). On the contrary, if we choose $6 < g^{min} < 32$ nS, g_{MS} decreases until it reaches the boundary and the system remains in the AS regime. This means that AS is only stable for appropriated boundaries.

Finally, we applied STDP in a PD regime (see Fig 1(d)). Without STDP, the period of the slave is 14.5 ms. After the plasticity is switched on, the system reaches a different PD regime. The slave period is 14.1 ms and the synaptic weight g_{MS} oscillates between 0 and 4 nS. The oscillation period of g_{MS} is $T \simeq 294$ ms which is almost 20 times the neuron period and it is related to the STDP time scales.

In the absence of STDP, the time delay τ between M and S is a smooth function of g_{MS} [7], which is shown in Fig 1(e). Note that, as mentioned, larger values of g_{MS} provide larger τ. The three different situations reported above were obtained by selecting different initial values of

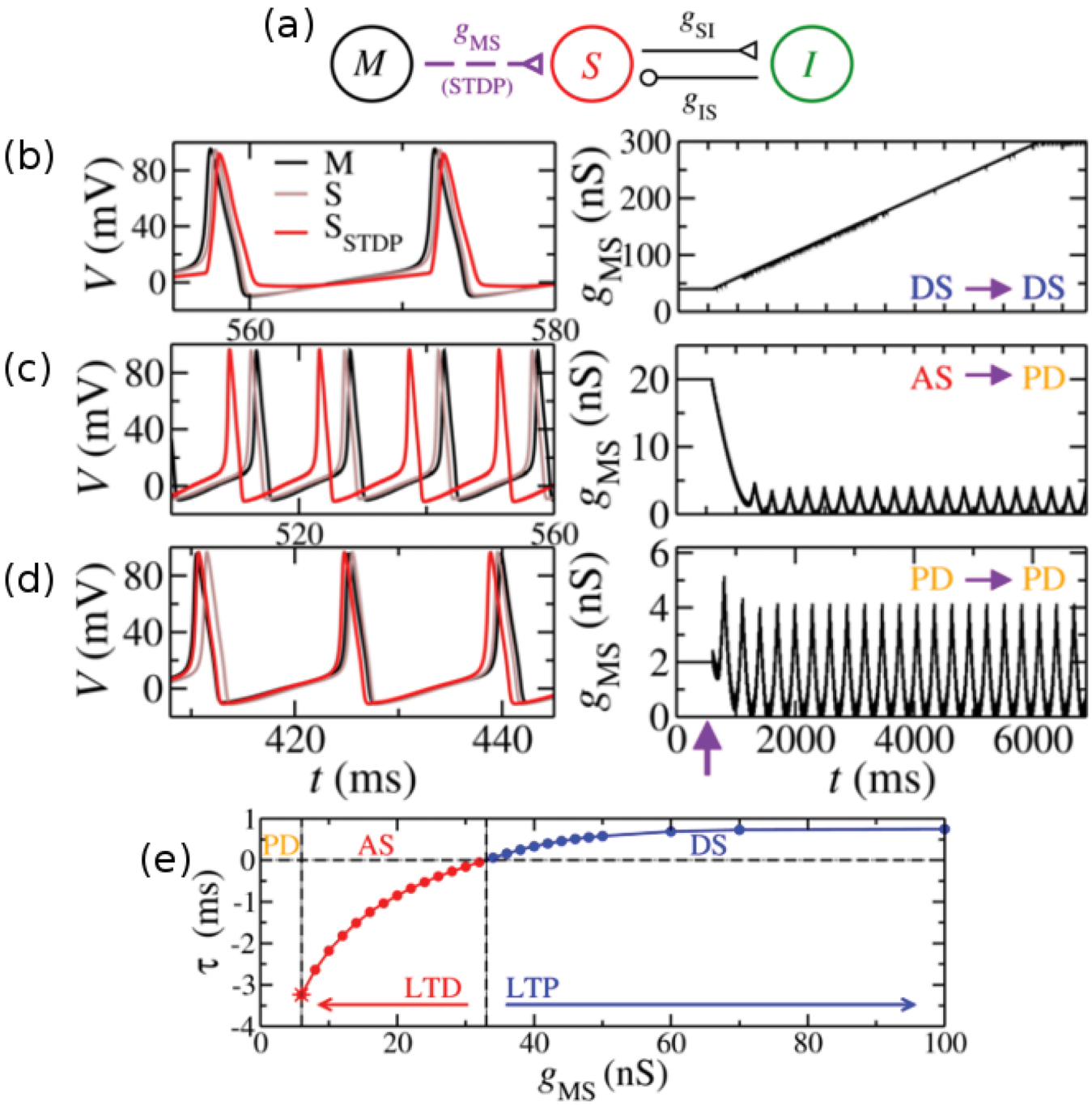

Fig 1. STDP in a microcircuit of three neurons. (a) Three neurons coupled by chemical synapses in the master-slave-interneuron (MSI) configuration. The excitatory synaptic weight g_{MS} may change through STDP rules. (b)-(d) Left: membrane potential of the master (M, black), the slave with no plasticity (S, grey) and the slave with STDP (S_{STDP}, red). Right: The synaptic weight g_{MS} as a function of time. The vertical arrow indicates the moment at which plasticity rules were switched on. The system can exhibit synchronized regimes with positive time delay (delayed synchronization, DS) or negative time delay (anticipated synchronization, AS) and a phase-drift (PD) regime. (b) The system initiates in the DS regime and remains in it. The synaptic weight increases from the initial value to the upper boundary. (c) The system initiates in the AS regime, then g_{MS} decreases to values smaller than 6 nS and the phase-drift (PD) regime is reached. (d) The system initiates in the PD regime and ends in a different PD regime. (e) Without STDP, the time delay τ between M and S is a smooth function of the weight g_{MS}. If we turn on STDP, the DS region (g_{MS} > 32 nS) leads to LTP whereas the AS region (6 < g_{MS} < 32 nS) leads to LTD. For g_{MS} < 6 nS the system exhibits a PD regime.

doi:10.1371/journal.pone.0140504.g001

the synaptic weight: g_{MS} = 40 nS (DS), g_{MS} = 20 nS (AS) and g_{MS} = 2 nS (PD). As expected, when we apply STDP rules in the AS regime the synaptic weight g_{MS} decreases by LTD, while in a DS regime, g_{MS} increases by LTP (see arrows in Fig 1(e)). If the system remains in a phase-locking regime (due to the boundaries), the final time-delay τ is determined by the final weight. In a nutshell, the presence of STDP in the 3-neuron motif takes the system close to the imposed boundaries of the STDP and far from the zero-lag synchronization solution.

Neuronal populations

Synchronization is robust against STPD. In order to extend our results to a cortical-like region, we investigate the effects of STDP in a population model which can exhibit AS [8]. We numerically studied the synchronization properties of two populations composed of hundred of neurons, described by the Izhikevich model, unidirectionally coupled in a master-slave configuration (see Fig 2(a) and Methods for more details). Neurons from the Master (M) population project excitatory synapses (each one with synaptic weight g_{MS}) to excitatory neurons from Slave-Interneuron (SI) population. The inhibitory loop that is mediated by the interneuron in the 3-neuron motif, is mediated by the inhibitory neurons inside the SI population. Thus, we assume that the slave population is composed by two subgroups: the excitatory neurons, called the Slave (S) sub-population, and the inhibitory neurons, called the Interneuron (I) sub-population. Each inhibitory synapse from I to S has synaptic weight g_{IS}. Without plasticity rules, the populations can oscillate with a well defined mean period [8]. Moreover, their activity can synchronize and the mean time delay τ between the M and S populations can be positive (DS) or negative (AS, see Methods). Similarly to the 3-neuron motif, τ is a continuous and smooth function of the synaptic weights g_{MS} and g_{IS}.

Here we investigate the effects of STDP only in the synapses from M to S allowing each synaptic weight g_{MS} to change according to the plasticity rules (see Eq 11 in the Methods section). After a transient time, the system reaches a synchronized regime. The mean membrane potential of the M and S populations are illustrated in Fig 2(b) and 2(c) for the AS and DS regimes respectively. In the AS regime the Slave precedes the Master, whereas in DS the Slave lags behind the Master. Due to the external noise and neuronal variability, the time delay in each period τ_i fluctuates around its mean value τ (see Fig 2(d) and 2(e) and Methods for more details).

Although synchronized oscillations are collective phenomena, the DS and AS regimes can also be represented at the neuronal level. The raster plots in Fig 3(a)–3(d) illustrate the oscillatory behavior of the coupled populations. Black (red) dashed lines indicate the time of peak average activity of the Master (Slave-Interneuron) population (see Methods for more details). In the DS regime the darker regions in the Slave-Interneuron population occur shortly after the ones in the Master population (see Fig 3(a) and 3(b)). On the contrary, in the AS regime, the darker regions in the Slave-Interneuron population occur before the ones in the Master population (see Fig 3(c) and 3(d)). However, there is a fraction of the neurons in the Master population which spikes before the peak of the Slave-Interneuron activity. The histograms in Fig 3(e) show the probability density of spike-timing intervals between each spike from neurons in the S population and the nearest spike from their respective pre-synaptic neurons in the M population. Although there are positive and negative values for the spike-timing intervals in both regimes, the peak and the mean of the distribution have positive values in the DS regime (blue, g_{IS} = 16 nS) and negative values in the AS regime (red, g_{IS} = 4 nS).

STDP promotes near-zero-lag synchronization. The presence of plasticity and the inhibitory dynamical loop can lead unidirectionally coupled neuronal populations to self-organize into near-zero-lag oscillations. The continuous transition from DS to AS, mediated by the excitatory synaptic weights g_{MS} in the absence of STDP, collapses into a flat line in the presence of

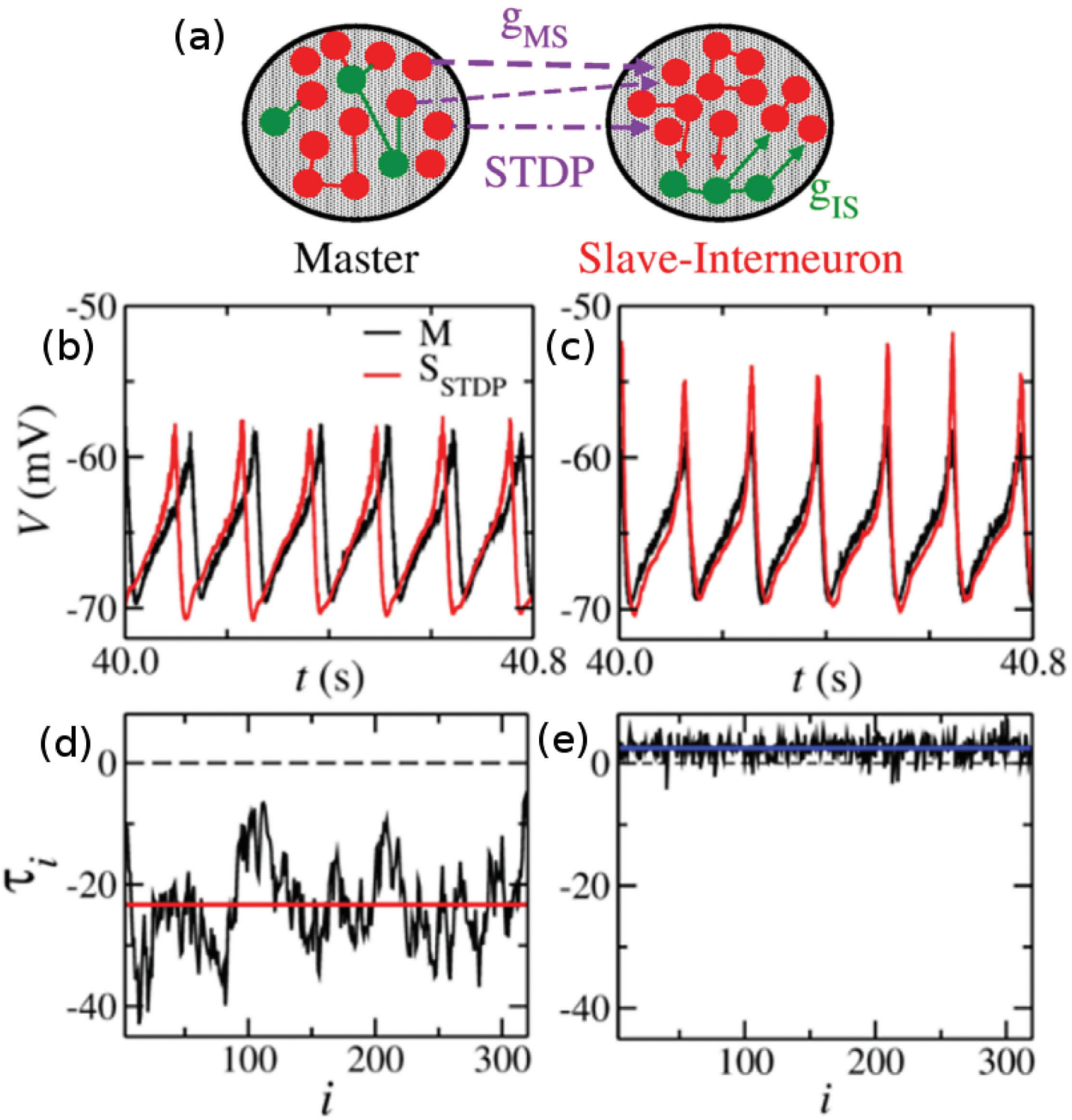

Fig 2. The interplay between phase difference and STDP in neuronal populations. (a) Master and Slave-Interneuron cortical-like populations. Each synaptic weight g_{MS} (from Master to the Slave) is subject to STDP rules. (b)-(c) Membrane potentials of M (black) and S (red) populations in the AS regime (b) and in the DS regime (c) in the presence of plasticity. (d)-(e) The time delay in each cycle τ_i. The mean time delay τ (flat line) is negative in the AS regime (d) and positive in the DS regime (e). The AS and DS regimes are obtained modifying only one parameter in the model. The inhibitory conductances in the Slave-Interneuron population is set to g_{IS} = 4 nS in the AS regime (b) and (d), whereas g_{IS} = 16 nS in the DS regime (c) and (e).

doi:10.1371/journal.pone.0140504.g002

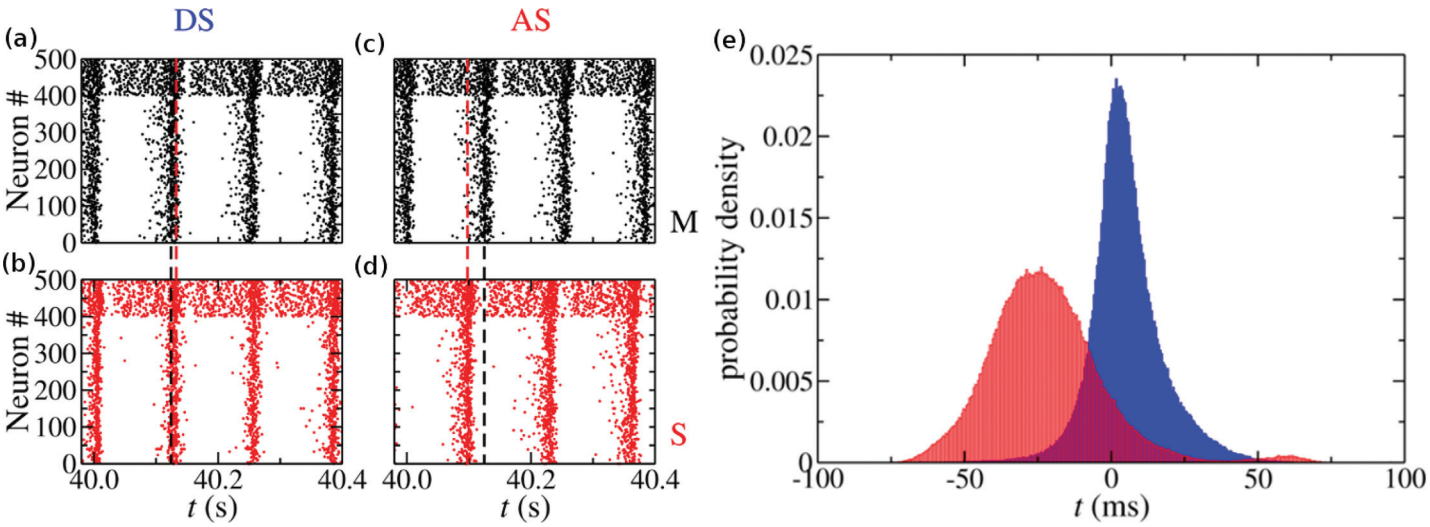

Fig 3. Neuronal firing patterns in the DS and AS regimes due to STDP. (a)-(d) Raster plots of each population in the DS and AS regimes. Black dots are neurons from the Master population. Red dots are neurons from the Slave-Interneuron population. Neurons 0 to 399 are excitatory, whereas neurons 400 to 499 are inhibitory. (e) Histogram of the time delay between the closest spikes in each cycle of all coupled pairs whose pre-synaptic neuron is in the M population and the post-synaptic neuron is in the S population. The blue distribution represents a DS regime and the red distribution represents an AS regime. The inhibitory conductances in the S population is set to g_{IS} = 16 nS in the DS regime, and g_{IS} = 4 nS in the AS regime.

doi:10.1371/journal.pone.0140504.g003

STDP (see Fig 4(a)–4(c)). For 7 nS $< g_{IS} <$ 12 nS the system exhibits time delay $\tau \simeq 0$ (see Fig 4 (h)). This means that independently of the initial values of the excitatory weights, the inhibitory loop together with STDP rules are sufficient to provide a $\tau \approx 0$ synchronized solution.

Despite the time decay of the chemical synapses, the neuronal variability and the external noise, the network exhibits $\tau \approx 0$ synchronized solution for a large set of parameters. For large enough Poisson rate ($R >$ 3500 Hz in our simulations, see Methods) the STDP rule brings the system closer to zero-lag synchronization (see Fig 5(a)). Although the conductance value of each individual synapse g_{MS} can change in time, the near-zero-lag regime is stable. In fact, in the near-zero-lag regime, the standard deviation of τ ($\approx$ 1.5 ms, see Fig 4(a)–(c)) is much smaller than the mean period of each population ($\approx$ 130 ms, see Fig 2(b) and 2(c)). Altogether, these results reveal a new mechanism which may contribute to the large-scale synchronization phenomena in the brain.

Interestingly, the result of the interplay between STDP and the collective oscillations cannot, in general, be predicted by analyzing the phase diagram without plasticity (Fig 4(g)). Assuming that all the synapses could be roughly described by a mean value, one could consider, for instance, the region 7 nS$\lesssim gIS \lesssim$ 16 nS (white arrows in Fig 4(g)). For low initial values of g_{MS}, below the zero-lag transition region, the system is in the DS regime, in principle leading STDP to increase the excitatory synaptic conductances. For larger, intermediate initial values of g_{MS}, the system is in the AS regime, which would lead STDP to reduce excitatory synaptic weights. Both conditions would push the system toward the zero-lag region, as is indeed observed in Fig 4(h) (although for a narrower interval of g_{IS} values). However, for even larger values of g_{MS} the system is again in the DS regime (Fig 4, orange arrow). Applying the same logic, one would expect STDP to increase g_{MS} even further, pushing the system away from the zero-lag regime. This is not verified in the simulations, suggesting that the actual STDP rule, which acts separately in each synapse, promotes a more robust synchronized regime than the one that would be reached if all synapses were identical.

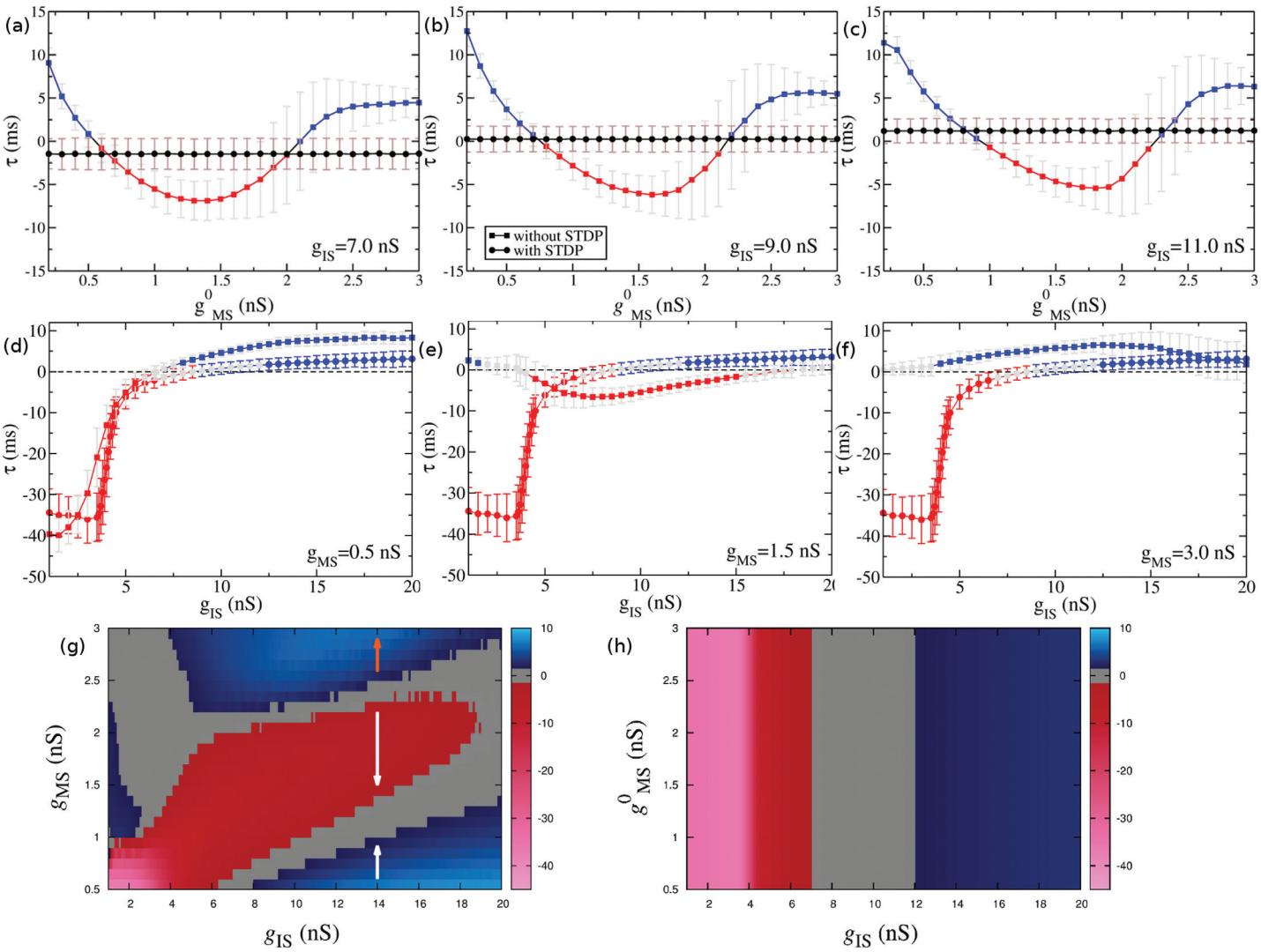

Fig 4. STDP changes the relation between the time delay τ and the synaptic weights. STDP promotes zero-lag synchronization ($\tau \approx 0$): (a)-(c) τ as a function of the initial excitatory weights g^0_{MS} with and without STDP (represented by circles and squares, respectively). (d)-(f) τ as a function of the inhibitory weights g_{IS} with and without STDP. (g)-(h) τ (color coded) in the (g_{IS}, g^0_{MS}) parameter space without plasticity (g) and with STDP (h). The near-zero-lag regime is represented by the grey regions, AS ($\tau < 0$) by the red regions and DS ($\tau > 0$) by the blue ones. In the presence of STDP, τ is determined by the local amount of inhibition g_{IS}.

doi:10.1371/journal.pone.0140504.g004

Anticipated synchronization as an emergent property. In Fig 4(d)–4(f) we show the relationship between τ and the inhibitory weights g_{IS} with and without plasticity in the excitatory conductance g_{MS}. In the presence of STDP, the time delay resists to change for inhibitory weights $g_{IS} < 4$ nS. However, when increasing g_{IS} beyond 4 nS, τ rapidly increases to near-zero values. Unlike the 3-neuron situation, in the cortical-like networks it is possible to start in a DS regime (without plasticity) and reach an AS regime via STDP or vice versa. The model also predicts that it is possible to start in an AS regime (or in a DS regime) and remains in AS (or DS) when STDP is turned on. In Fig 4(g) and 4(h) we compare the values of τ along the parameter space (g_{IS}, g^0_{MS}) with and without plasticity. Without STDP, the combination of g_{MS} and g_{IS} that provides positive or negative τ is non trivial as shown in Fig 4(g). This means that STDP acts as an organizing mechanism for the network. For fixed STDP parameters there is a well-defined

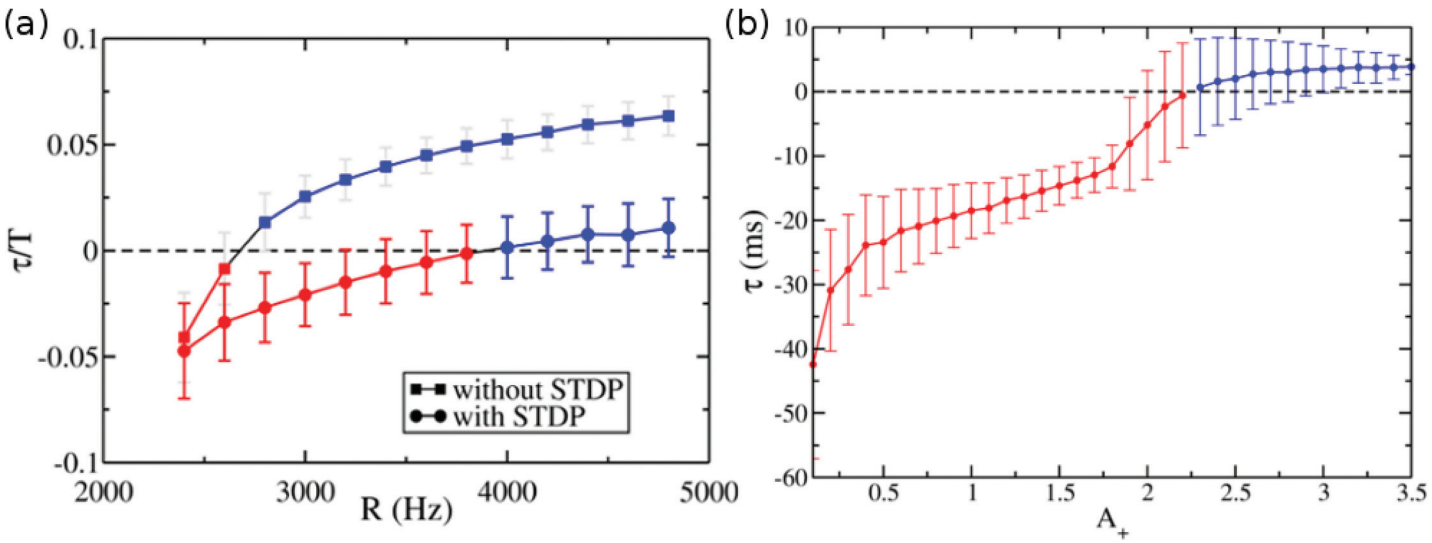

Fig 5. Robustness of synchronization regimes against model parameters. (a) Effect of external noise with and without plasticity: time delay normalized to the period of the Master population τ/T versus the Poisson rate R of the external noise. The inhibitory conductances in the Slave-Interneuron population is g_{IS} = 5 nS and A_+ = 0.5. (b) Time delay τ versus the parameter of the STDP rule A_+ (see Eq 11) for g_{IS} = 4 nS. A smooth transition from AS to DS can be observed.

doi:10.1371/journal.pone.0140504.g005

and continuous region of negative, positive and near-zero time delay synchronized solutions (see Fig 4(h)). Furthermore, with and without STDP, the time delay can be modulated by the amount of external noise, which could switch on or off the anticipation (see Fig 5(a)) Interestingly, the presence of plasticity allows the AS regime to persist for larger noise values and be robust to the parameters tat govern the STDP.

The transition from AS to DS is continuous and smooth when changing the parameters A_+ and A_- in Eq 11. Fig 5(b) shows the relationship between τ and A_+ for fixed A_- = 1.0. In fact, our model not only illustrates an example of AS in the presence of STDP but also shows that STDP enlarges the parameter region in which the time delay is negative.

STDP and negative phase difference stabilize synaptic weight distribution. A remarkable outcome of our model is related to the synaptic weight distribution when the system reaches an AS regime via STDP. As a result of the dynamical interaction between AS and STDP, the weight distribution obeys the three key properties required for biophysical reliability [46] as shown in Fig 6(a). First, the shape of the distribution is stable. Although each synapse can individually change in time, the distribution of all synaptic weights maintains a similar pattern along time. Second, it is diverse; it does not concentrate all the values at the boundaries. Third, it is limited i.e. there are no infinitely large synapses. More interestingly, synaptic weights do not explode even without an arbitrarily chosen boundary.

On the contrary, for a DS regime, the third property is not completely satisfied. Eventually it is necessary to choose an upper boundary for the weights, otherwise some of them grow beyond biophysical limits. In Fig 6(a) we see that there is a probability of finding arbitrarily large values of g_{MS} in the DS regime in the absence of a boundary, which does not happen for AS regime. However, the stability of the weights' distribution and diversity of weights still occur. In Fig 6(b) we see the evolution of four randomly chosen synaptic weights starting from different initial conditions in the AS and DS regimes. In the DS regime there is a probability of extremely fast growing of the synaptic weights. On the contrary, in the AS regime all weights converge to small values. It is worth mentioning that these results do not depend on the initial values of g_{MS}.

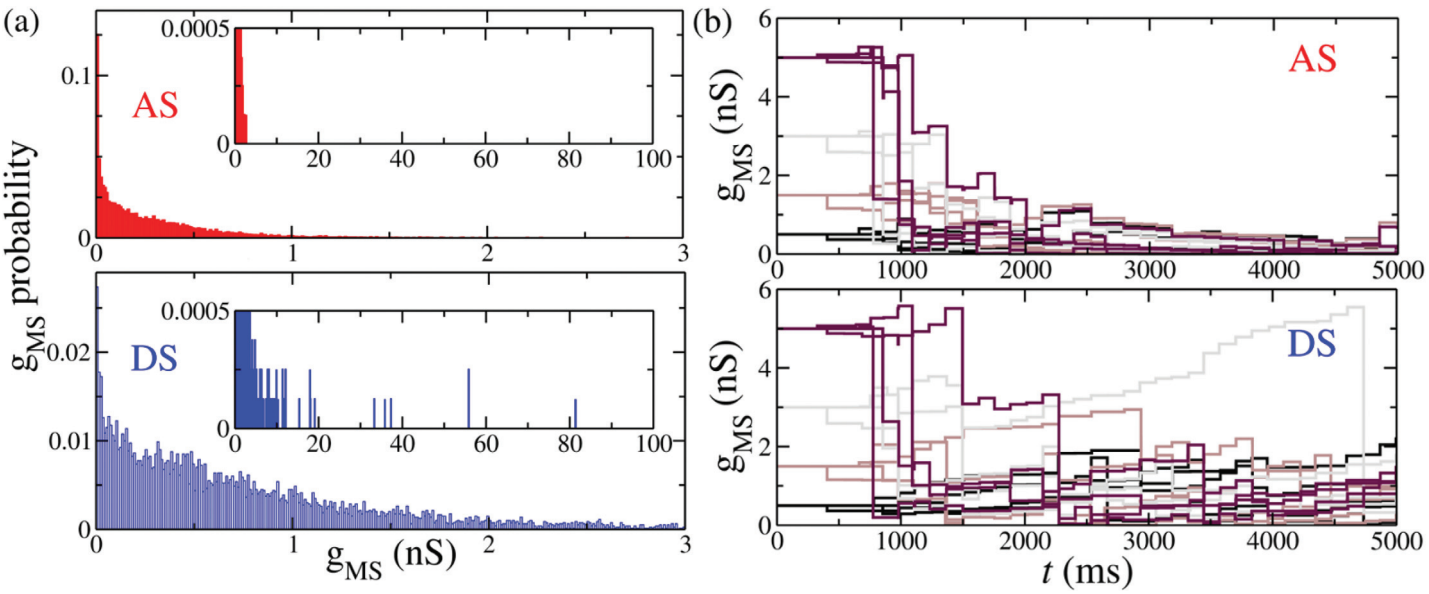

Fig 6. Synaptic weight distributions in the presence of STDP rules. (a) Histogram of the g_{MS} values. Inset: AS provides limited weight distribution even without an upper boundary. However, in the DS regime some synapses can grow unlimited. (b) Time evolution of four randomly chosen synaptic weights starting from different initial conditions in the AS and DS regimes. Each color represents a different simulation in which all initial synaptic conductances g^0_{MS} were the same. The inhibitory conductances in the Slave-Interneuron population is g_{IS} = 4 nS in the AS regime, while g_{IS} = 16 nS in the DS regime.

doi:10.1371/journal.pone.0140504.g006

Discussion

It is known that depending on the relative spike timing, synaptic weights can be modified through STDP mechanisms [37]. Moreover, previous works have shown how synaptic changes in the coupling of neural systems can impact their synchronization regimes, inverting the time lag [7, 8]. In the present paper we have investigated how the interplay between STDP and the synchronization regimes dynamically control the network function and connectivity.

In the population model, STDP acts at the synaptic level between each pair of pre-post synaptic neurons, whereas the synchronization time τ between the two populations is influenced by all g_{MS} values, reflecting a collective behavior. Therefore, the presence of plasticity could, in principle, hamper the synchronization. However the synergetic interplay between STDP and the AS-DS transition provides robust and stable synchronized regimes. We have shown that the AS regime is stable in a large set of parameter values in the presence of STDP rules. Moreover, due to the STDP the AS-DS transition is independent of the initial values of the excitatory weights. Consequently, the time delay can be controlled by the local amount of inhibition at the receiver population. For instance, if the Master population projects unidirectional synapses to two distinct slave populations, the phase difference between the two uncoupled slave population would depend on the strength in the local inhibitory pool.

Master-Slave populations self-organizes into near-zero-lag synchronization

Zero-lag synchronization has been extensively studied in the brain. It was first reported in cat visual cortex [50], but has been widely found in neuronal functions, ranging from perceptual integration to the execution of motor behaviors [3, 51–54]. From the modeling viewpoint, several mechanisms have been pointed out as partially responsible for the enhancement of such synchrony. Among many, we can cite inhibitory synapses and gap junctions [55, 56], a

canonical circuit of excitatory and inhibitory neurons for the hippocampal neurons [57–59] and synaptic plasticity mechanisms [60].

More recently, a robust mechanism, named dynamical relaying, has been proposed [61, 62] and tested in the thalamo-cortical [63] and hippocampal [64] circuits. The model proposes that two spatially separated areas can synchronize at zero lag if they are mutually coupled through a third area placed between them. The mechanism was found to be robust for certain parameters range, in the presence of inhomogeneity [62, 65], for modified motifs [66] and against STDP rules [39, 59, 67]. Here we show that STDP rules can also promote zero-lag synchronization in unidirectionally coupled motifs. Our results provide a new motif, different from those proposed in the dynamical relaying scenario, which allows near-zero-lag synchronization between distant cortical areas. Furthermore, we show that the zero-lag regime is stable, robust and can be controlled by the inhibitory synapses in the receiver region.

Plasticity yields robust weight distributions and synchronized regimes

There have been several attempts to answer the question of how weight distributions and synaptic plasticity rules are related [45, 47, 48, 68, 69]. Typically, the experimental synaptic weight distributions reported in the literature have similar shapes: a monotonic decay function with maximum probability near zero, but different scales [47]. In addition, plenty of studies (in the cortex, hippocampus, and cerebellum) strongly suggest the existence of a large majority of undetectable synapses with almost zero weight. In our model, AS can shape the weight distributions between the Master and Slave populations into biophysical plausible patterns [47]. Such distributions present a monotonic decay and obey three key properties [46]: they are stable, diverse and limited (see Fig 6(a)).

Furthermore, a negative time delay could facilitate the responsiveness of post-synaptic neurons. For example, the olfactory receptor neurons (ORNs) and the projection neurons (PNs) of male moths are unidirectionally coupled. Interestingly, it has been verified that the response time of the PNs is smaller than the one of the ORNs [70]. Rospars et al. [70] have suggested that this shorter latency of PNs could be explained by AS. Since the PNs exhibit a multiphasic response pattern with an initial excitation followed by an inhibition, they could be subject to a similar dynamical inhibitory loop as the one required for AS.

Several works support that communication between brain regions is more efficient at near zero-lag synchronization [53, 54, 71]. However, an explanation for the underlying mechanisms and the functional significance of the reported phase differences between cortical regions [6, 9, 72–75] is still lacking. Although it is often assumed that the phase difference between distant areas reflects the transmission time of neural activity [73, 74, 76], it has been shown that, for the same given directional influence, the phase difference can be positive, negative or near zero [6, 8, 9]. Here we have shown that STDP does not destroy these synchronization regimes, but rather makes them more robust, and, in principle, tunable by local inhibition.

Methods

The master-slave-interneuron microcircuit

The typical master-slave configuration consists of two neurons unidirectionally coupled by an excitatory synapse. Here we have studied the 3-neuron motif illustrated in Fig 1. The circuit is composed by a master-slave coupling and a dynamical inhibitory loop mediated by an interneuron [7]. Each neuron is described by a Hodgkin-Huxley model [77], which consists of four coupled ordinary differential equations associated to the membrane potential V and the ionic currents flowing across the axonal membrane corresponding to the Na^+, K^+ and leakage currents. The gating variables for sodium are h and m and for the potassium is n. The equations

are [78]:

$$C_m \frac{dV}{dt} = \bar{G}_{Na} m^3 h (E_{Na} - V) + \bar{G}_K n^4 (E_K - V) + G_m (V_{rest} - V) + I + \sum I_{syn} \quad (1)$$

$$\frac{dx}{dt} = \alpha_x(V)(1-x) - \beta_x(V)x \,, \quad (2)$$

where $x \in \{h, m, n\}$, $C_m = 9\pi\ \mu$F is the membrane capacitance of a $30\times30\times\pi\ \mu m^2$ equipotential patch of membrane [78] and $\sum I_{syn}$ accounts for the synapses from other neurons. The external constant current $I = 280$ pA settles the period of the neuron as $T = 14.7$ ms for $\sum I_{syn} = 0$. The reversal potentials are $E_{Na} = 115$ mV, $E_K = -12$ mV and $V_{rest} = 10.6$ mV, with maximal conductances $\bar{G}_{Na} = 1080\pi$ mS, $\bar{G}_K = 324\pi$ mS and $G_m = 2.7\pi$ mS, respectively.

The excitatory and inhibitory synapses are modulated by AMPA (A) and $GABA_A$ (G). The fraction $r^{(i)}$ ($i = A,G$) of bound synaptic receptors is modeled by:

$$\frac{dr^{(i)}}{dt} = \alpha_i [T](1 - r^{(i)}) - \beta_i r^{(i)}, \quad (3)$$

The values of the rate constants are $\alpha_A = 1.1$ mM^{-1}ms^{-1}, $\beta_A = 0.19$ ms^{-1}, $\alpha_G = 5.0$ mM^{-1}ms^{-1}, and $\beta_G = 0.30$ ms^{-1}. $[T]$ is the neurotransmitter concentration in the synaptic cleft, given by:

$$[T](V_{pre}) = \frac{T_{max}}{1 + e^{[-(V_{pre} - V_p)/K_p]}}, \quad (4)$$

where $T_{max} = 1$ mM^{-1}, $K_p = 5$ mV and $V_p = 62$ mV. The synaptic current at a given synapse is given by

$$I^{(i)} = g_i r^{(i)} (E_i - V), \quad (5)$$

where V is the postsynaptic potential, $E_A = 60$ mV and $E_G = -20$ mV are the reversal potentials. The maximal weight g_i in the excitatory synapse from M to S (called g_{MS}) and in the inhibitory synapse from I to S (called g_{IS}) are the important parameters of our model. Particularly, g_{MS} can be modified by STDP rules, as explained below. The existence of an AS regime specially depends on g_{IS} [7]. Here we use $g_{IS} = 40$ nS. The excitatory synaptic weight from S to I is fixed $g_{SI} = 40$ nS, but our results are almost independent of its specific value. We use fourth order Runge-Kutta's method for numerical integrations with a time step of 0.01 ms. Simulations were performed using a C++ code which is available upon request.

Modeling cortical-like neuronal populations

The two unidirectionally coupled neuronal networks in Fig 2 might represent cortical regions in the brain [62]. Each population is composed of hundreds of neurons described by the Izhikevich model [79] given by:

$$\frac{dv}{dt} = 0.04v^2 + 5v + 140 - u + \sum I_x, \quad (6)$$

$$\frac{du}{dt} = a(bv - u). \quad (7)$$

where v is the membrane potential and u the recovery variable, which account for activation of K^+ and inactivation of Na^+ ionic currents. The currents in $\sum I_x$ represent the synaptic currents.

If $v \geq 30$mV, then v is reset to c and u to $u + d$. For each excitatory neuron: $(a, b) = (0.02, 0.2)$ and $(c, d) = (-65, 8) + (15, -6)\sigma^2$, whereas for each inhibitory neuron: $(a, b) = (0.02, 0.25) + (0.08, -0.05)\sigma$ and $(c, d) = (-65, 2)$. σ is a random variable uniformly distributed on the interval [0, 1] which determines the proportion of different neurons (regular spiking, intrinsically bursting, chattering—including type I and II excitability).

The excitatory (AMPA) and inhibitory ($GABA_A$) synaptic current are mediated by:

$$I_x = g_x r_x (E_x - v), \tag{8}$$

where $x = A,G$, $E_A = 0$ mV and $E_G = -65$ mV. Unless otherwise stated all excitatory (inhibitory) weights are set to $g_A = 0.5$ ms ($g_G = 4$ nS). The dynamics of the fraction of bound synaptic receptors r_x is given by:

$$\tau_x \frac{dr_x}{dt} = -r_x + \sum_k \delta(t - t_k). \tag{9}$$

The summation over k stands for pre-synaptic neurons. The time decays are $\tau_A = 5.26$ ms and $\tau_G = 5.6$ ms. Each neuron receives an independent Poisson input, representing n pre-synaptic neurons spiking with rate R/n. The noise mimics excitatory chemical synapses from other brain regions. The rate R strongly influences the main oscillation frequency of each population. We use Euler's method with a time step of 0.05 ms to integrate the differential equations.

The Master (M) population is composed of 500 neurons (80% excitatory, 20% inhibitory), each one receiving 50 synapses (sparse connectivity $\approx$ 10%) from randomly selected neighbors (excitatory or inhibitory) in the same population. For an external rate $R = 2400$ Hz, the mean membrane potential V of this population oscillates with a mean period $T_M \approx 130$ ms, corresponding to a frequency $f \approx 7.7$ Hz, which is related to theta oscillations reported in several experiments [53, 74, 75].

The Slave-Interneuron population is also composed of 500 neurons. In order to maintain the analogy with the 3-neuron motif we called Slave (S) population the sub-group of 400 excitatory neurons and Interneuron (I) population the sub-group of 100 inhibitory neurons belonging to the cortical-like Slave-Interneuron network. Each excitatory neuron from the S population receives 40 excitatory synapses from neighbor neurons belonging to S, 20 synapses from excitatory neurons from the M population (g_{MS}, which characterizes the master-slave coupling) and 10 synapses from the interneurons in the I population (with conductances g_{IS}, which play the role of the delayed self-feedback responsible for AS). Only the excitatory synaptic weights g_{MS} evolve under STDP rules.

Each neuron from the I population receives 10 inhibitory synapses from randomly selected neighbors neurons belonging to the same I population and 40 excitatory synapses from randomly selected neurons belonging to the S population. Results are quantitatively similar if we measure the mean membrane potential of just the S population or the S and I populations together. In fact, for all set of parameters employed here, S and I are synchronized. Then, the S and I populations can be considered as sub-populations of the same cortical region or well separated regions in the brain oscillating with the same frequency.

We use a sliding window (from 5 to 8 ms) to decrease the noise effect and to determine the time of the membrane peak in each period t_i^x (x = M,S,I index the population and i the period). In all calculations we discount a transient time of 10 s and run the simulation until $t = 50$ s. The period of each population in each cycle is given by $T_i^x \equiv t_{i+1}^x - t_i^x$ and we calculate the mean period T_x and its variance. Similarly, the time delay in each cycle is defined as $\tau_i = t_i^S - t_i^M$. Then we obtain the mean time delay τ and its standard deviation, which is plotted as the error bars in Figs 4 and 5.

STDP between unidirected coupled networks

In the 3-neuron motif the g_{MS} synaptic weight evolves under the additive rule:

$$\Delta g = \begin{cases} A_+ \exp(-t/\tau_+), & \text{if } t > 0 \\ -A_- \exp(t/\tau_-), & \text{if } t < 0, \end{cases} \tag{10}$$

with $A_+ = A_- = 1$ nS, $\tau_+ = \tau_- = 10$ ms and artificial boundaries $0 < g_{MS} < 300$ nS.

For the populations, each excitatory synaptic weight g_{MS} from the Master to the Slave is subject to the following hybrid rule [80]:

$$\Delta g = \begin{cases} A_+ \exp(-t/\tau_+), & \text{if } t > 0 \quad \text{(additive LTP)} \\ -A_- g \exp(t/\tau_-), & \text{if } t < 0 \quad \text{(multiplicative LTD)} \end{cases} \tag{11}$$

where $t = t^S - t^M$. It is worth mentioning that if we use an additive rule to LTD, it is necessary to choose a lower boundary for g_{MS} in order to avoid negative weights. Unless otherwise stated $\tau_+ = \tau_- = 5$ ms, $A_+ = 0.5$ nS, $A_- = 1.0$ and there are no arbitrarily chosen boundaries.

Acknowledgments

This work was supported by project FIS2012-30634 (Intense@cosyp) from Ministerio de Economia y Competitividad, Espaa and Fondo Europeo de Desarrollo Regional. Coordenação de Aperfeiçoamento de Pessoal de Nível Superior (CAPES, Brazilian project Ciência Sem Fronteiras PVE 88881.068077/2014-01); Conselho Nacional de Desenvolvimento Científico e Tecnológico (CNPq), Fundação de Amparo à Ciência e Tecnologia do Estado de Pernambuco (FACEPE), special programs as Programa de Apoio a Núcleos Emergentes (PRONEM) and FAPESP Center for Neuromathematics (grant # 2013/07699-0, S. Paulo Research Foundation FAPESP). The funders had no role in study design, data collection and analysis, decision to publish, or preparation of the manuscript.

Author Contributions

Analyzed the data: FM PC CM MC. Wrote the paper: FM PC CM MC. Performed the simulations: FM. Analyzed the results: FM PC CM MC. Discussed results: FM PC CM MC.

References

1. Buzsaki G. Rhythms of the Brain. Oxford University Press (New York); 2006.
2. Wang XJ. Neurophysiological and Computational Principles of Cortical Rhythms in Cognition. Physiological Reviews. 2010; 90:1195–1268. doi: 10.1152/physrev.00035.2008 PMID: 20664082
3. Uhlhaas PJ, Pipa G, Lima B, Melloni L, Neuenschwander S, Nikolić D, et al. Neural synchrony in cortical networks: history, concept and current status. Front Integr Neurosci. 2009; 3:17. doi: 10.3389/neuro.07.017.2009 PMID: 19668703
4. Miltner W, Braun C, Arnold M, Witte H, Taub E. Coherence of gamma-band EEG activity as a basis for associative learning. Nature. 1999; 397:434–436. doi: 10.1038/17126 PMID: 9989409
5. Fell J, Axmacher N. The role of phase synchronization in memory processes. Nature Reviews Neuroscience. 2011; 12:105–118. doi: 10.1038/nrn2979 PMID: 21248789
6. Salazar RF, Dotson NM, Bressler SL, Gray CM. Content-Specific Fronto-Parietal Synchronization During Visual Working Memory. Science. 2012; 338:1097–1100. doi: 10.1126/science.1224000 PMID: 23118014
7. Matias FS, Carelli PV, Mirasso CR, Copelli M. Anticipated synchronization in a biologically plausible model of neuronal motif. Phys Rev E. 2011; 84:021922. doi: 10.1103/PhysRevE.84.021922
8. Matias FS, Gollo LL, Carelli PV, Bressler SL, Copelli M, Mirasso CR. Modeling positive Granger causality and negative phase lag between cortical areas. NeuroImage. 2014; 99:411–418. doi: 10.1016/j.neuroimage.2014.05.063 PMID: 24893321

9. Brovelli A, Ding M, Ledberg A, Chen Y, Nakamura R, Bressler SL. Beta oscillations in a large-scale sensorimotor cortical network: Directional influences revealed by Granger causality. Proc Natl Acad Sci USA. 2004; 101(26):9849–9854. doi: 10.1073/pnas.0308538101 PMID: 15210971
10. Voss HU. Anticipating Chaotic Synchronization. Phys Rev E. 2000; 61:5115. doi: 10.1103/PhysRevE.61.5115
11. Voss HU. Dynamic Long-Term Anticipation of Chaotic States. Phys Rev Lett. 2001; 87(1):014102. PMID: 11461468
12. Voss HU. Erratum: Anticipating chaotic synchronization [Phys. Rev. E 61, 5115 (2000)]. Phys Rev E. 2001; 64(3):039904. doi: 10.1103/PhysRevE.64.039904
13. Ciszak M, Mirasso CR, Toral R, Calvo O. Predict-prevent control method for perturbed excitable systems. Phys Rev E. 2009; 79(4):046203. doi: 10.1103/PhysRevE.79.046203
14. Mayol C, Mirasso CR, Toral R. Anticipated synchronization and the predict-prevent control method in the FitzHugh-Nagumo model system. Phys Rev E. 2012; 85:056216. doi: 10.1103/PhysRevE.85.056216
15. Masoller C, Zanette DH. Anticipated synchronization in coupled chaotic maps with delays. Physica A. 2001; 300(3-4):359–366. doi: 10.1016/S0378-4371(01)00362-4
16. Kostur M, Hänggi P, Talkner P, Mateos JL. Anticipated synchronization in coupled inertial ratchets with time-delayed feedback: A numerical study. Phys Rev E. 2005; 72(3):036210. doi: 10.1103/PhysRevE.72.036210
17. Che Y, Li R, Han C, Cui S, Wang J, Wei X, et al. Topology identification of uncertain nonlinearly coupled complex networks with delays based on anticipatory synchronization. Chaos. 2013; 23:013127. doi: 10.1063/1.4793541 PMID: 23556964
18. Sivaprakasam S, Shahverdiev EM, Spencer PS, Shore KA. Experimental Demonstration of Anticipating Synchronization in Chaotic Semiconductor Lasers with Optical Feedback. Phys Rev Lett. 2001; 87(15):154101. doi: 10.1103/PhysRevLett.87.154101 PMID: 11580702
19. Tang S, Liu JM. Experimental Verification of Anticipated and Retarded Synchronization in Chaotic Semiconductor Lasers. Phys Rev Lett. 2003; 90:194101. doi: 10.1103/PhysRevLett.90.194101 PMID: 12785948
20. Pisarchik AN, Jaimes-Reategui R, Garcia-Lopez H. Synchronization of coupled bistable chaotic systems: experimental study. Phil Trans R Soc A. 2008; 366:459–473. doi: 10.1098/rsta.2007.2103 PMID: 17681912
21. Liu Y, Takiguchi Y, Davis P, Aida T, Saito S, M LJ. Experimental observation of complete chaos synchronization in semiconductor lasers. Appl Phys Lett. 2002; 80(23):4306. doi: 10.1063/1.1485127
22. Corron NJ, Blakely JN, Pethel SD. Lag and anticipating synchronization without time-delay coupling. Chaos. 2005; 15:023110. doi: 10.1063/1.1898597
23. Senthilkumar DV, Lakshmanan M. Transition from anticipatory to lag synchronization via complete synchronization in time-delay systems. Phys Rev E. 2005 Jan; 71:016211. doi: 10.1103/PhysRevE.71.016211
24. Pyragas K, Pyragienè T. Coupling design for a long-term anticipating synchronization of chaos. Phys Rev E. 2008; 78:046217. doi: 10.1103/PhysRevE.78.046217
25. Blakely JN, Pruitt MW, Corron NJ. Time shifts and correlations in synchronized chaos. Chaos. 2008; 18:013117. doi: 10.1063/1.2840778 PMID: 18377068
26. Ambika G, Amritkar RE. Anticipatory synchronization with variable time delay and reset. Phys Rev E. 2009 May; 79:056206. doi: 10.1103/PhysRevE.79.056206
27. Xu S, Yang Y, Song L. Control-oriented approaches to anticipating synchronization of chaotic deterministic ratchets. Phys Lett A. 2009; 373:2226–2236. doi: 10.1016/j.physleta.2009.03.028
28. Pyragienè T, Pyragas K. Anticipating spike synchronization in nonidentical chaotic neurons. Nonlinear Dynamics. 2013; 74(1-2):297–306. doi: 10.1007/s11071-013-0968-7
29. Pyragienè T, Pyragas K. Anticipating chaotic synchronization via act-and-wait coupling. Nonlinear Dynamics. 2015; 79:1901–1910. doi: 10.1007/s11071-014-1782-6
30. Ciszak M, Calvo O, Masoller C, Mirasso CR, Toral R. Anticipating the Response of Excitable Systems Driven by Random Forcing. Phys Rev Lett. 2003; 90:204102. doi: 10.1103/PhysRevLett.90.204102 PMID: 12785899
31. Stepp N, Turvey MT. On strong anticipation. Cognitive Systems Research. 2010; 11(2):148–164. doi: 10.1016/j.cogsys.2009.03.003 PMID: 20191086
32. Stephen DG, Dixon JA. Coordinate-independent Mapping of Structural and Functional Data by Objective Relational Transformation (ORT). Chaos, Solitons and Fractals. 2011; 44:160–168.

33. Sausedo-Solorio J, Pisarchik A. Synchronization of map-based neurons with memory and synaptic delay. Physics Letters A. 2014; 378(30):2108–2112. doi: 10.1016/j.physleta.2014.05.003

34. Simonov AY, Gordleeva SY, Pisarchik A, Kazantsev V. Synchronization with an arbitrary phase shift in a pair of synaptically coupled neural oscillators. JETP letters. 2014; 98(10):632–637. doi: 10.1134/S0021364013230136

35. Markram H, Lübke J, Frotscher M, Sakmann B. Regulation of synaptic efficacy by coincidence of postsynaptic APs and EPSPs. Science. 1997; 275(5297):213–5. doi: 10.1126/science.275.5297.213 PMID: 8985014

36. Bi GQ, Poo MM. Synaptic modifications in cultured hippocampal neurons: dependence on spike timing, synaptic strength, and postsynaptic cell type. The Journal of Neuroscience. 1998; 18(24):10464–72. PMID: 9852584

37. Markram H, Gerstner W, Sjöström PJ. A history of spike-timing-dependent plasticity. Frontiers in Synaptic Neuroscience. 2011; 3(0004):1–24.

38. Nowotny T, Zhigulin VP, Selverston AI, Abarbanel HD, Rabinovich MI. Enhancement of synchronization in a hybrid neural circuit by spike-timing dependent plasticity. The Journal of Neuroscience. 2003; 23(30):9776–9785. PMID: 14586005

39. Knoblauch A, Hauser F, Gewaltig MO, Körner E, Palm G. Does spike-timing-dependent synaptic plasticity couple or decouple neurons firing in synchrony? Frontiers in Computational Neuroscience. 2012; 6:55. doi: 10.3389/fncom.2012.00055 PMID: 22936909

40. Zhigulin VP, Rabinovich MI, Huerta R, Abarbanel HD. Robustness and enhancement of neural synchronization by activity-dependent coupling. Phys Rev E. 2003; 67(2):021901. doi: 10.1103/PhysRevE.67.021901

41. Lubenov EV, Siapas AG. Decoupling through Synchrony in Neuronal Circuits with Propagation Delays. Neuron. 2008; 58(1):118–131. doi: 10.1016/j.neuron.2008.01.036 PMID: 18400168

42. Cassenaer S, Laurent G. Hebbian STDP in mushroom bodies facilitates the synchronous flow of olfactory information in locusts. Nature. 2007; 448(7154):709–713. doi: 10.1038/nature05973 PMID: 17581587

43. Takahashi YK, Kori H, Masuda N. Self-organization of feed-forward structure and entrainment in excitatory neural networks with spike-timing-dependent plasticity. Phys Rev E. 2009 May; 79:051904. doi: 10.1103/PhysRevE.79.051904

44. Gerstner W, Van Hemmen JL, Cowan JD. What matters in neuronal locking? Neural Computation. 1996; 8(8):1653–1676. doi: 10.1162/neco.1996.8.8.1653 PMID: 8888612

45. Song S, Miller KD, Abbott LF. Competitive Hebbian learning through spike-timing-dependent synaptic plasticity. Nature Neuroscience. 2000; 3(9):919–926. doi: 10.1038/78829 PMID: 10966623

46. Burbank KS, Kreiman G. Depression-biased reverse plasticity rule is required for stable learning at top-down connections. PLoS Computational Biology. 2012; 8(3):e1002393. doi: 10.1371/journal.pcbi.1002393 PMID: 22396630

47. Barbour B, Brunel N, Hakim V, Nadal JP. What can we learn from synaptic weight distributions? TRENDS in Neurosciences. 2007; 30(12):622–629. doi: 10.1016/j.tins.2007.09.005 PMID: 17983670

48. Song S, Sjöström PJ, Reigl M, Nelson S, Chklovskii DB. Highly nonrandom features of synaptic connectivity in local cortical circuits. PLoS Biology. 2005; 3(3):e68. doi: 10.1371/journal.pbio.0030068 PMID: 15737062

49. Lefort S, Tomm C, Sarria JCF, Petersen CC. The excitatory neuronal network of the C2 barrel column in mouse primary somatosensory cortex. Neuron. 2009; 61(2):301–316. doi: 10.1016/j.neuron.2008.12.020 PMID: 19186171

50. Gray CM, König P, Engel AK, Singer W, et al. Oscillatory responses in cat visual cortex exhibit intercolumnar synchronization which reflects global stimulus properties. Nature. 1989; 338(6213):334–337. doi: 10.1038/338334a0 PMID: 2922061

51. Roelfsema PR, Engel AK, König P, Singer W. Visuomotor Integration is Associated with Zero Time-Lag Synchronization Among Cortical Areas. Nature. 1997; 385:157–161. doi: 10.1038/385157a0 PMID: 8990118

52. Singer W. Neuronal Synchrony: A versatile Code for the Definition of Relations? Neuron Review. 1999; 24:49–65. doi: 10.1016/S0896-6273(00)80821-1

53. Varela F, Lachaux JP, Rodriguez E, Martinerie J. The Brainweb: Phase Synchronization and large-scale integration. Nature Reviews Neuroscience. 2001; 2:229–239. doi: 10.1038/35067550 PMID: 11283746

54. Fries P. A mechanism for cognitive dynamics: neuronal communication through neuronal coherence. Trends in Cognitive Sciences. 2005; 9(10):474–480. doi: 10.1016/j.tics.2005.08.011 PMID: 16150631

55. Van Vreeswijk C, Abbott L, Ermentrout GB. When inhibition not excitation synchronizes neural firing. Journal of Computational Neuroscience. 1994; 1(4):313–321. doi: 10.1007/BF00961879 PMID: 8792237

56. Kopell N, Ermentrout B. Chemical and electrical synapses perform complementary roles in the synchronization of interneuronal networks. Proc Natl Acad Sci USA. 2004; 101(43):15482–15487. doi: 10.1073/pnas.0406343101 PMID: 15489269

57. Traub RD, Whittington MA, Stanford IM, Jefferys JG. A mechanism for generation of long-range synchronous fast oscillations in the cortex. Nature. 1996; 383:621–624. doi: 10.1038/383621a0 PMID: 8857537

58. Ermentrout GB, Kopell N. Fine structure of neural spiking and synchronization in the presence of conduction delays. Proc Natl Acad Sci USA. 1998; 95(3):1259–1264. doi: 10.1073/pnas.95.3.1259 PMID: 9448319

59. Knoblauch A, Sommer FT. Synaptic plasticity, conduction delays, and inter-areal phase relations of spike activity in a model of reciprocally connected areas. Neurocomputing. 2003; 52:301–306. doi: 10.1016/S0925-2312(02)00792-0

60. Kopell N, Ermentrout G, Whittington M, Traub R. Gamma rhythms and beta rhythms have different synchronization properties. Proc Natl Acad Sci USA. 2000; 97(4):1867–1872. doi: 10.1073/pnas.97.4.1867 PMID: 10677548

61. Fischer I, Vicente R, Buldú JM, Peil M, Mirasso CR, Torrent M, et al. Zero-lag long-range synchronization via dynamical relaying. Phys Rev Lett. 2006; 97(12):123902. doi: 10.1103/PhysRevLett.97.123902 PMID: 17025966

62. Vicente R, Gollo LL, Mirasso CR, Fischer I, Pipa G. Dynamical relaying can yield zero time lag neuronal synchrony despite long conduction delays. Proc Natl Acad Sci USA. 2008; 105(44):17157–17162. doi: 10.1073/pnas.0809353105 PMID: 18957544

63. Gollo LL, Mirasso C, Villa AEP. Dynamic control for synchronization of separated cortical areas through thalamic relay. Neuroimage. 2010; 52:947–955. doi: 10.1016/j.neuroimage.2009.11.058 PMID: 19958835

64. Gollo LL, Mirasso CR, Atienza M, Crespo-Garcia M, Cantero JL. Theta band zero-lag long-range cortical synchronization via hippocampal dynamical relaying. PLoS One. 2011; 6:e17756. doi: 10.1371/journal.pone.0017756 PMID: 21408082

65. Esfahani ZG, Valizadeh A. Zero-Lag Synchronization Despite Inhomogeneities in a Relay System. PLoS One. 2014; 9(12):e112688. doi: 10.1371/journal.pone.0112688

66. Gollo LL, Mirasso C, Sporns O, Breakspear M. Mechanisms of zero-lag synchronization in cortical motifs. PLoS Computational Biology. 2014; 10(4):e1003548. doi: 10.1371/journal.pcbi.1003548 PMID: 24763382

67. Viriyopase A, Bojak I, Zeitler M, Gielen S. When long-range zero-lag synchronization is feasible in cortical networks. Frontiers in Computational Neuroscience. 2012; 6:49. doi: 10.3389/fncom.2012.00049 PMID: 22866034

68. Nathan A, Barbosa VC. Network algorithmics and the emergence of the cortical synaptic-weight distribution. Phys Rev E. 2010; 81(2):021916. doi: 10.1103/PhysRevE.81.021916

69. Iyer R, Menon V, Buice M, Koch C, Mihalas S. The Influence of Synaptic Weight Distribution on Neuronal Population Dynamics. PLoS Computational Biology. 2013; 9(10):e1003248. doi: 10.1371/journal.pcbi.1003248 PMID: 24204219

70. Rospars JP, Grémiaux A, Jarriault D, Chaffiol A, Monsempes C, Deisig N, et al. Heterogeneity and Convergence of Olfactory First-Order Neurons Account for the High Speed and Sensitivity of Second-Order Neurons. PLoS Computational Biology. 2014; 10(12):e1003975. doi: 10.1371/journal.pcbi.1003975 PMID: 25474026

71. Abeles M. Local Cortical Circuits: An Electrophysiological study. Springer (Berlin); 1982.

72. Dotson NM, Salazar RF, Gray CM. Frontoparietal Correlation Dynamics Reveal Interplay between Integration and Segregation during Visual Working Memory. The Journal of Neuroscience. 2014; 34(41):13600–13613. doi: 10.1523/JNEUROSCI.1961-14.2014 PMID: 25297089

73. Gregoriou GG, Gotts SJ, Zhou H, R D. High-Frequency, Long Range Coupling Between Prefrontal and Visual Cortex During Attention. Science. 2009; 324:1207–1210. doi: 10.1126/science.1171402 PMID: 19478185

74. Liebe S, Hoerzer GM, Logothetis NK, Rainer G. Theta coupling between V4 and prefrontal cortex predicts visual short-term memory performance. Nature Neuroscience. 2012; 15(3):456–462. doi: 10.1038/nn.3038 PMID: 22286175

75. Phillips JM, Vinck M, Everling S, Womelsdorf T. A long-range fronto-parietal 5-to 10-Hz network predicts top-down? controlled guidance in a task-switch paradigm. Cerebral Cortex. 2014; 24(8):1996–2008. doi: 10.1093/cercor/bht050 PMID: 23448872

76. Sharott A, Magill PJ, Bolam JP, Brown P. Directional analysis of coherent oscillatory field potentials in the cerebral cortex and basal ganglia of the rat. The Journal of Physiology. 2005; 562:951–963. doi: 10.1113/jphysiol.2004.073189 PMID: 15550466

77. Hodgkin AL, Huxley AF. A Quantitative Description of Membrane Current and Its Application to Conduction and Excitation in Nerve. The Journal of Physiology. 1952; 117:500–544. doi: 10.1113/jphysiol.1952.sp004764 PMID: 12991237

78. Koch C. Biophysics of Computation. New York: Oxford University Press; 1999.

79. Izhikevich EM. Simple model of spiking neurons. IEEE Transaction on Neural Networks. 2003; 14(6):1569. doi: 10.1109/TNN.2003.820440

80. Billings G, van Rossum MCW. Memory retention and spike-timing-dependent plasticity. Journal of Neurophysiology. 2009; 101(6):2775–2788. doi: 10.1152/jn.91007.2008 PMID: 19297513